ACS OMEGA

Article

Cite This: ACS Omega 2018, 3, 6066−6074

Targeting of a Photosensitizer to the Mitochondrion Enhances the Potency of Photodynamic Therapy

Sakkarapalayam M. Mahalingam,[†,‡,⊥] Josue D. Ordaz,[†,§,⊥,∥] and Philip S. Low*[,†,‡]

[†]Department of Chemistry and [‡]Institute for Drug Discovery, Purdue University, 720 Clinic Drive, West Lafayette, Indiana 47907, United States

[§]Indiana University School of Medicine, 340 W 10th Street #6200, Indianapolis, Indiana 46202, United States

Supporting Information

ABSTRACT: Photodynamic therapy (PDT) involves use of a photosensitizer, whose activation with light leads to the production of singlet oxygen (SOS), generation of reactive oxygen species (ROS), and initiation of associated cell toxicity. Because a cell's mitochondria constitute sites where oxygen levels are high, ROS can be readily produced, and apoptosis is commonly initiated. Therefore, an ideal PDT agent might be a potent photosensitizer that could naturally accumulate in mitochondria. Although a number of mitochondria-targeting moieties, including triphenylphosphine, guanidinium, and bisguanidium, have been identified, a quantitative comparison of their efficacies in targeting mitochondria has not been performed. In this study, we have prepared triphenylphosphine, guanidinium, and bisguanidium derivatives of the FDA-approved PDT agent verteporfin (Visudyne, benzoporphyrin derivative-monoacid ring A: **BPD-MA**) and compared their abilities to induce the intracellular perturbations common to potent PDT agents. Cellular parameters examined included subcellular localization of the verteporfin, real-time monitoring of SOS production, quantitation of reactive oxygen species (ROS) generation, analysis of mitochondria and chromatin integrity, characterization of cytoskeletal disruption and evaluation of cytochrome *C* release as a measure of apoptosis. An analysis of these parameters demonstrates that the triphenylphosphine derivative (**0323**) has better mitochondria-targeting efficacy, SOS production, and mitochondria membrane toxicity than either unmodified verteporfin or its guanidinium derivatives. Consistent with this potency, **0323** also induced the most prominent mitochondria swelling, actin depolymerization, pyknosis, and cytochrome *C* release. We conclude that triphenylphosphine has a better mitochondria-targeting moiety than guanidinium or bis-guanidinium and those PDT photosensitizers with improved cytotoxicities can be prepared by conjugating a mitochondria-targeting moiety to the desired photosensitizer.

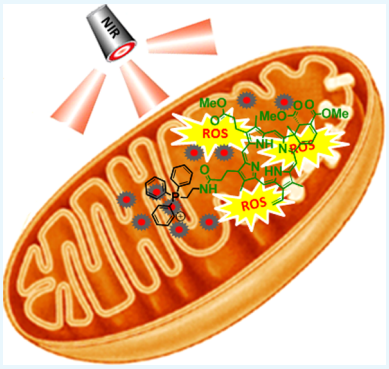

INTRODUCTION

Photodynamic therapy (PDT) combines light energy, oxygen, and a light-absorbing molecule called a photosensitizer to induce an oxidative stress in the illuminated (usually neoplastic) cells.[1] Each of these components is nontoxic by itself, but, when combined, can induce a chain of reactions leading to the production of reactive oxygen species (ROS) causing cell death. The photosensitizer (PS) is a molecule that can absorb a photon that excites an outer shell electron to a singlet state (S_1), which can then either return to its ground state (i.e., by fluorescence or heat emission) or undergo intersystem crossing to a triplet state,[2] which can then react with oxygen to generate free radicals (type I reaction) or singlet oxygen species (type II reaction). These reactive oxygen species then undergo a series of downstream reactions to cause oxidative damage.[3]

One of the challenges in photodynamic therapy (PDT) is to develop novel photosensitizers that can improve the therapeutic efficacy without imposing undesirable requirements for prolonged/enhanced exposure to activating light. The major parameter used to compare the potencies of different photosensitizers is singlet oxygen quantum yield (ϕ_Δ), which is the efficiency by which a photosensitizer uses light energy to convert molecular oxygen to singlet oxygen.[4] Photosensitizers that contain the highest ϕ_Δ are desirable because singlet oxygen is a powerful oxidant that can directly induce cellular toxicity. However, it has been demonstrated that a direct correlation between singlet oxygen production and cell death does not exist, but rather the toxicity of PDT depends on the subcellular localization of the PDT agent.[5] Because singlet oxygen is highly reactive and readily quenched (its lifetime is of the order of 40 ns and its diffusion radius is ∼20 nm[6]), its site of production will almost certainly be its site of oxidative damage (i.e., a mammalian cell's diameter is of the order of ∼10−30 μm and mitochondria organelles are ∼900 nm wide).[7] The solution, if achievable, would be to target a PDT agent specifically to an organelle where SOS/ROS could be efficiently produced and the toxic effects of SOS/ROS would be sensitively experienced. Based on the reports that mitochondria contain high

Received: April 10, 2018
Accepted: May 23, 2018
Published: June 5, 2018

DOI: 10.1021/acsomega.8b00692
ACS Omega 2018, 3, 6066−6074

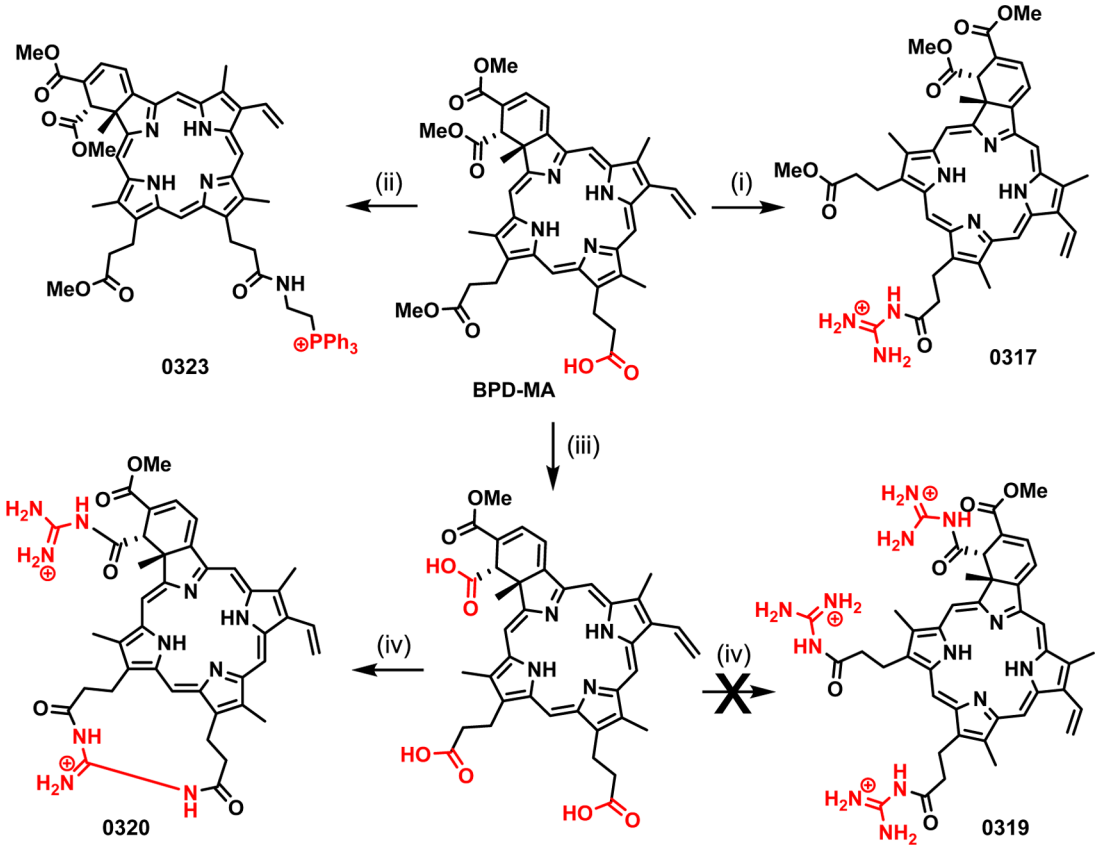

Figure 1. Synthesis of the modified verteporfin to target mitochondria. Reagents and conditions: (i) HATU, diisopropylethylamine (DIPEA), dimethyl sulfoxide (DMSO), room temperature (r.t.) 30 min then guanidine (2 equiv) stir overnight, (ii) HATU, DIPEA, DMSO, r.t. 25 min then (2-aminoethyl)triphenylphosphonium bromide (2 equiv) stir overnight, (iii) Me_3SnOH (10 equiv), 1,2-DCE, 80 °C, 1 h, (iv) HATU, DIPEA, DMSO, r.t. 30 min then guanidine (6 equiv) stir overnight.

concentrations of oxygen[9] and that even low levels of singlet oxygen produced in the mitochondria are more toxic than large amounts produced in the nucleus,[8] it seemed logical to try to develop a photosensitizer that would target the mitochondria. Additional observations that the mitochondria are decisive regulators of apoptosis and that these organelles produce most of the cell's energy only added motivation to this objective.[10,11] Indeed, most of the clinically approved photosensitizers including Foscan,[12] Photofrin,[13] and Visudyne[14] already partially localize to the mitochondria.

Methods to improve mitochondria targeting have included conjugation of such mitochondria-targeting moieties as guanidinium, bisguanidinium, or triphenylphosphine groups to the main compound to introduce a delocalized positive charge and increase the compound's lipophilicity, which collectively are thought to increase a conjugate's affinity for mitochondria. A previous study by Sibrian-Vazquez et al. showed an increased localization of porphyrin compounds to the mitochondria upon synthesizing their guanidinium and bisguanidinium derivatives.[15] Although these guanidinium and bisguanidinium were shown to localize to the mitochondria, the modified compounds were never compared to the parent compound, making it unclear whether these molecules actually increased mitochondria localization. Triphenylphosphine group is another extensively studied mitochondria-targeting moiety that has been used for the delivery of chemotherapeutics,[16−19] antioxidants,[20] imaging probes,[21] photosensitizers,[22−24] and other molecules.[25] However, to our knowledge, there has not been a comparison of these moieties in their mitochondria-targeting efficiencies.

Herein, we present a multimodal comparison of the PDT agent, verteporfin, with three of its mitochondria-targeted derivatives in a human head and neck cancer cell line. The compound verteporfin was chosen because it was already known to partially concentrate in mitochondria, which if increased upon conjugation to guanidinium, bisguanidinium, or triphenylphosphine would provide a robust test of the value of mitochondrial targeting for maximization of PDT potency. Moreover, verteporfin is an FDA-approved drug for the treatment of wet age-related macular degeneration[26,27] and has a longer absorption wavelength than the other mitochondria-targeting photosensitizers mentioned above, which is desirable to target deeper tissue.

RESULTS AND DISCUSSION

The molecules synthesized for this study included **0317**, which contains monoguanidinium group in the carboxyl terminus; **0320**, which contains a cyclic bis-guanidinium group that bridges the carboxyl termini; and **0323**, which contains a triphenylphosphine group on the carboxyl terminus (Figure 1). As shown in Figure 1, the monoacid ring A of verteporfin was coupled to guanidine and (2-aminoethyl)-triphenylphosphonium bromide 2-(1*H*-7-azabenzotriazol-1-yl)-1,1,3,3-tetramethyl uronium hexafluorophosphate methanaminium (HATU) as a coupling agent to obtain the monoguanidinium and triphenylphosphonium derivative of

DOI: 10.1021/acsomega.8b00692
ACS Omega 2018, 3, 6066−6074

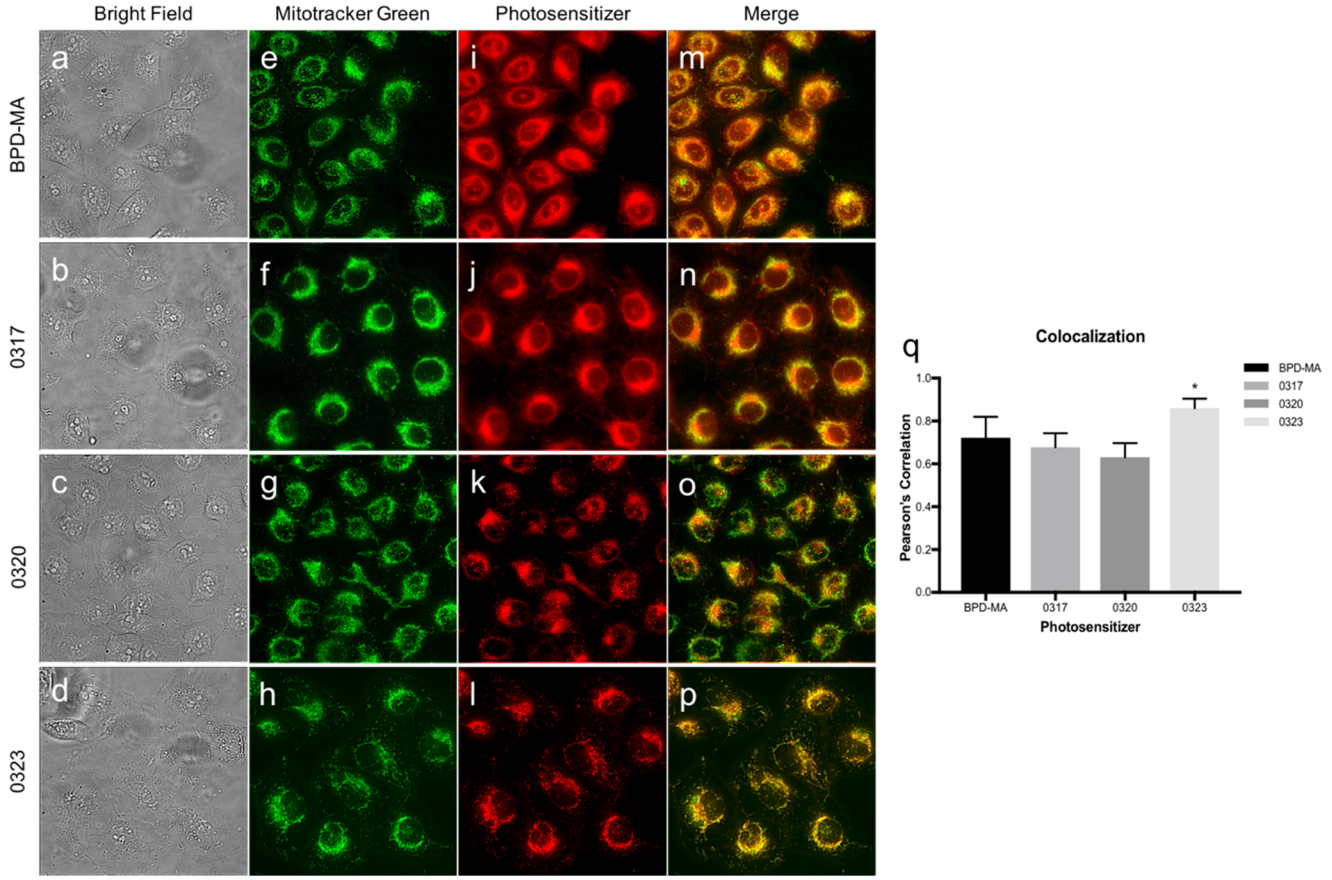

Figure 2. Localization of **BPD-MA** and modified compounds in the mitochondria. (a–d) Bright field images of human KB cells. Cells stained with Mitotracker green (e–h) and photosensitizers (i–l). (m–p) Merged image of green and red channels showing colocalization (yellow) of photosensitizers and Mitotracker green. (q) Modified compound **0323** showed a significantly higher colocalization compared to **BPD-MA** using Pearson's correlation coefficient and one-way ANOVA with Tukey's post-hoc test ($p = 0.0326$). $n = 5$ images for each group. $^*p < 0.05$. It should be noted that the photosensitizer fluorescence images do not correlate with the amount of compound intracellularly. These images were modified after capture to help the readers optimally visualize the intracellular localization of each compound. These adjustments have no effect on the calculation of colocalization because Pearson's Correlation Coefficient is independent of pixel intensity/brightness.

verteporfin named **0317** and **0323**, respectively. To achieve bis- and tris-guanidinium derivative of verteporfin for increased mitochondria-targeting, we tried the conventional methyl ester hydrolysis conditions to obtain di- and tri- free carboxylic acid derivative of verteporfin. However, our attempt with strong and mild basic conditions for methyl ester hydrolysis were unsuccessful, and we observed complex products in liquid chromatography–mass spectrometry (LCMS). Finally, we optimized using Me_3SnOH, which had been established by Nicolaou and co-workers[28] to hydrolyze selectively the aliphatic methyl esters without damaging the olephenic methyl ester in the E ring of verteporfin. To obtain a tris-guanidinium derivative of verteporfin, the tri-carboxylic acid derivative was further conjugated with guanidine using HATU coupling condition. The reaction was monitored by LCMS, and the major product shows the molecular weight of 755.2, which is not that of our expected tris-guanidinium derivative **0319** (MW: 816.9). The LCMS analysis indicates that the isolated product with the molecular weight of 755.2 was the cyclic bis-guanidinium derivative **0320**.

To compare these compounds, we quantified and compared their mitochondria localization, intracellular singlet oxygen production, and mitochondria membrane potential ($\Delta\psi_m$) change. Furthermore, we studied the morphological changes of the cytoskeleton and mitochondria and reactive oxygen species production. Because the goal of PDT is to kill pathological cells, cell death was analyzed by observing nuclear pyknosis and cytochrome *C* release from the mitochondria. Results from this study should facilitate the discovery and optimization of novel PDT therapeutics by determining which substituent will promote the most photosensitizer accumulation in the mitochondria. Moreover, the methods employed here should help guide development of newer photosensitizers by establishing methods to compare their efficacy.

Cellular Localization of Modified Compounds. The subcellular fate of the modified compounds was determined by fluorescent microscopy. Pearson's correlation coefficient was used to determine the localization of the photosensitizers (Figure 2i–l) in the mitochondria, which was labeled with Mitotracker green (Figure 2e–h). As shown in Figure 2, when the Mitotracker and **0323** fluorescence images were merged, a very strong colocalization signal was observed (Figure 2p). The calculated Pearson's correlation coefficients (±SEM) were 0.722 (± 0.044) for **BPD-MA**, 0.678 (± 0.029) for **0317**, 0.631 (± 0.029) for **0320**, and 0.860 (± 0.012) for **0323**. Using a one-way ANOVA with Tukey post-hoc test, the modified compound **0323** showed a significantly higher localization to the mitochondria than **BPD-MA** (p-value = 0.033), whereas the other modified compounds showed no difference compared to **BPD-MA**.

DOI: 10.1021/acsomega.8b00692
ACS Omega 2018, 3, 6066–6074

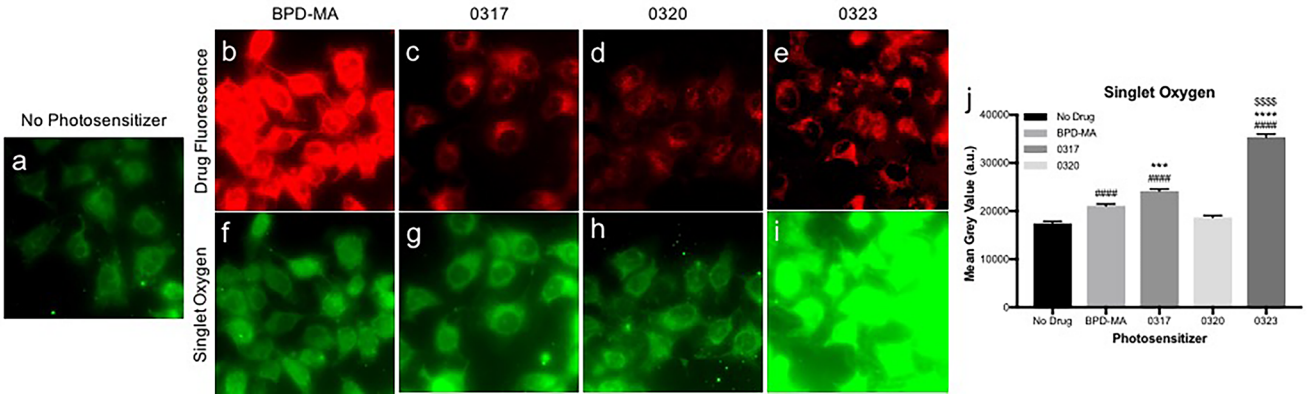

Figure 3. Intracellular singlet oxygen production after irradiation. (a) KB cells with no drug. (b–e) Fluorescence of photosensitizers and (f–i) corresponding intracellular singlet oxygen production. (j) Singlet oxygen quantification after light treatment shows statistically significant increase in **BPD-MA**-treated (p-value < 0.0001), **0317**-treated (p-value < 0.0001), and **0323**-treated (p-value < 0.0001) cells compared with no drug; **0317**-treated (p-value = 0.001) and **0323**-treated (p-value < 0.0001) compared to **BPD-MA**-treated cells; and **0323**-treated (p-value < 0.0001) compared with **0317**-treated cells. Statistics were done using one-way ANOVA with Tukey post-hoc analysis. n = 75 cells for all groups. # used for comparison with no drug, * for comparison with **BPD-MA** and $ for comparison with **0317**. ***p < 0.001, ****p < 0.0001. It should be noted, contrary to the previous figure, the postcapture parameters (i.e., LUTs) for the photosensitizer fluorescence images were constant in this figure to provide the viewer with a visual measure of the relative fluorescence of each molecule.

The results demonstrate that verteporfin (**BPD-MA**) localizes to the mitochondria, which agrees with earlier studies reporting its localization to the mitochondria of pancreatic cancer cells,[32] endothelial cells, and prostate cancer cells.[33] There was improved mitochondria targeting of **BPD-MA** by using the triphenylphosphine (TPP) moiety, which also agrees with the literature showing TPP as an effective mitochondria-targeting molecule.[24] Although guanidinium and biguanidinium have also been used to target the mitochondria, our results demonstrate that they reduced mitochondria localization of **BPD-MA**. The study by Sibrian-Vasquez et al., which showed an increased mitochondria localization, did not quantify the localization and compare the synthesized compounds to the unmodified porphyrins.[15] Because porphyrins naturally localize to the mitochondria, without comparison to an untargeted control porphyrin, it is difficult to draw any conclusion regarding the ability of an added substituent to improve mitochondria localization. Moreover, because **BPD-MA**, which is a porphyrin derivative, has already been shown to significantly localize in the mitochondria, further improvements may be difficult.

Singlet Oxygen Species Production. The effect of **BPD-MA** and its derivatives on intracellular singlet oxygen species generation was investigated. Previous studies have used singlet oxygen quantum yield to compare different photosensitizers. However, these values do not accurately predict the intracellular singlet oxygen production, which depends on the localization of the photosensitizer and its proximity to oxygen. Therefore, singlet oxygen sensor green (SOSG), which reacts with singlet oxygen to produce a highly fluorescent endoperoxide molecule, was used as a marker of intracellular singlet oxygen production.[34] Due to its low cellular penetrance as a consequence of extracellular protein binding, the method described by Choudhury et al. was used.[35] Higher intensity of SOSG fluorescence, which corresponds to an increase in the singlet oxygen species production, was observed in photosensitizer-treated cells (Figure 3f–i) compared to the nontreated control group (Figure 4a) following irradiation. To further determine the singlet oxygen production, fluorescence intensity was quantified[36] using ImageJ's mean gray value (n = 75 cells) (Figure 4j). There was significantly higher singlet oxygen production with **0317** (24 142 au ± 451.5) treatment compared to **BPD-MA** (21 072 au ± 423.1) treatment after light irradiation (p-value = 0.001) and with **0323** (35339 au ± 666) treated cells compared to verteporfin (p-value < 0.0001) and **0317** (p-value < 0.0001) treatment. Treatment with **0320** (18 674 au ± 405.5) did not show any difference from nontreated cells (17 456 au ± 442.4) (p-value = 0.3944).

We observe the highest production of singlet oxygen species after irradiation of **0323**-treated cells. From the previous colocalization experiments, it was shown that **0323** had the greatest accumulation in the mitochondria compared to the other photosensitizers. Because the mitochondria is an organelle with the highest intracellular oxygen concentration,[9] and because oxygen is required for PDT,[37] it was not surprising that the photosensitizer with the highest mitochondria localization also had the highest ROS production. It should also be noted that the excited state energy following near-infrared (NIR) illumination can be dissipated by multiple mechanisms, and that compounds that fluoresce efficiently are usually poor PDT agents and vice versa. Thus, compounds that efficiently convert excited state energy into emitted fluorescence must necessarily have less excited state energy available for the production of reactive oxygen species (i.e., via intersystem crossing, formation of singlet oxygen, and further reaction to generate other ROS). The fact that **0323** has the lowest fluorescence and highest ROS, whereas **BPD-MA** has the highest fluorescence and the lowest ROS is consistent with this explanation.

Changes in Mitochondria Membrane Potential. Singlet oxygen is highly reactive and damaging to membranes.[38] Thus, we hypothesized that the increased production of singlet oxygen in mitochondria will cause damage to its membranes. To test this hypothesis, we measured the mitochondria membrane potential ($\Delta\psi_m$) with the JC-1 assay. JC-1 is a cationic dye that accumulates in the mitochondria depending on the $\Delta\psi_m$.[39] During low $\Delta\psi_m$, low concentrations of JC-1 localize in the mitochondria, forming mostly monomers that emit green fluorescence. However, with higher $\Delta\psi_m$, there is an increased concentration of JC-1 in the mitochondria, leading to

DOI: 10.1021/acsomega.8b00692
ACS Omega 2018, 3, 6066–6074

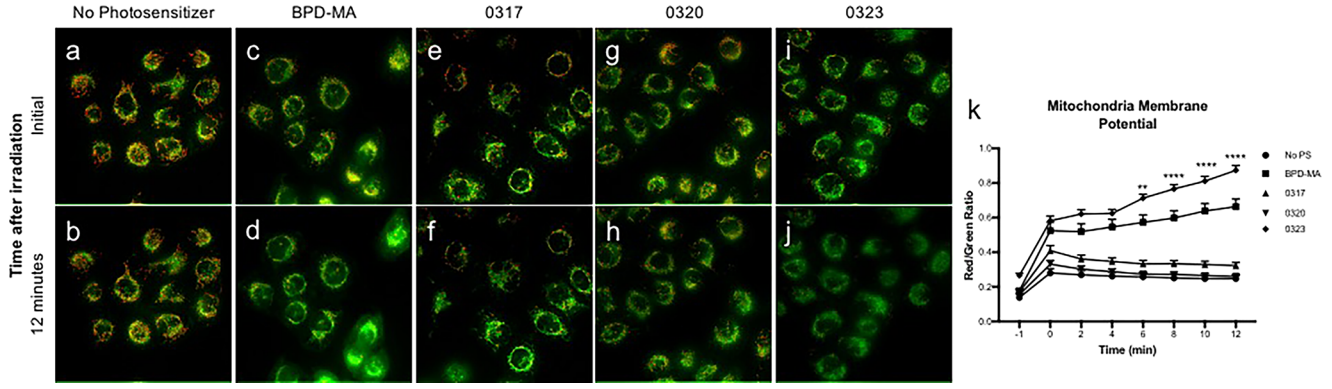

Figure 4. Changes in mitochondria membrane potential. JC-1 signal in control cells (a, b) and cells treated with **BPD-MA** (c, d), **0317** (e, f), **0320** (g, h), and **0323** (i, j) directly after (a–i) and 12 min (b–j) after irradiation. (k) Green-to-red channel ratio during longitudinal study for 12 min upon irradiation. Higher ratio corresponds to reduction in membrane potential. **0323**-treated cells show significant reduction in mitochondria membrane potential at 6 min ($p = 0.002$), 8 min ($p < 0.0001$), 10 min ($p < 0.0001$), and 12 min ($p < 0.0001$). Statistical analysis was done using 2-way ANOVA ($n = 20$ cells for time = −1 for all groups; $n = 30$ for nontreated group thereafter and $n = 40$ for photosensitizer groups). $^{**}p < 0.01$, $^{****}p < 0.0001$.

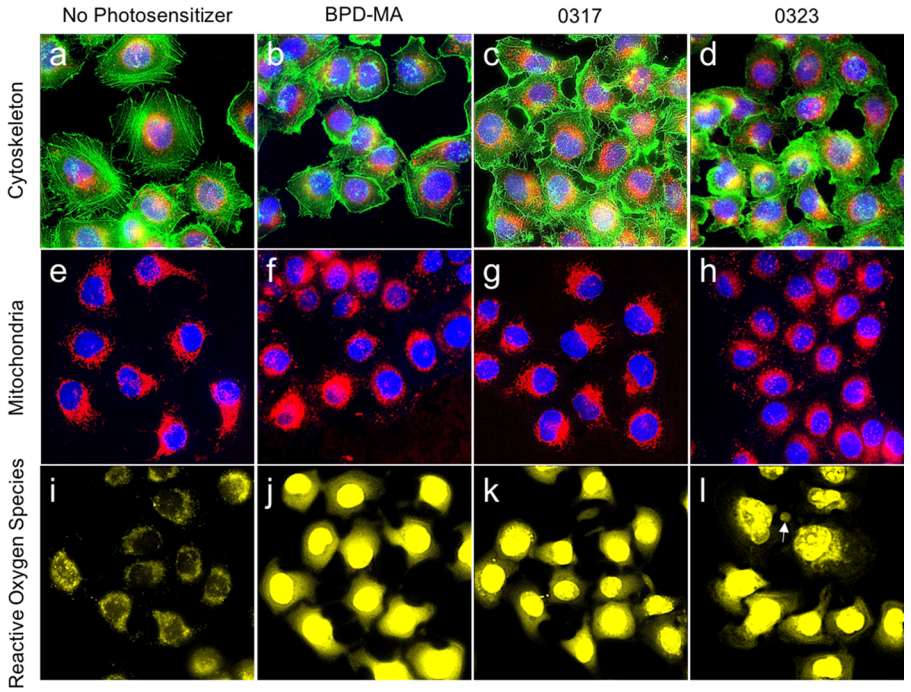

Figure 5. Qualitative changes observed in cytoskeleton, mitochondria morphology, and ROS following irradiation. (a–d) Actin cytoskeleton in nontreated cells and photosensitizer-treated cells. (e–h) Mitochondria morphology studies. (i–l) Changes in ROS production following light irradiation. (l) Apoptotic body indicated by the arrow.

the formation of JC-1 aggregates that emit red fluorescence. Quantitative analysis of $\Delta\psi_m$ was performed by ratiometric analysis[40] of green monomer (green channel) to red aggregate (red channel) (Figure 4k). The ratio of monomer to aggregate fluorescence was used as a surrogate for analyzing the $\Delta\psi_m$ change. Before light irradiation, no difference between control and photosensitizer groups was observed, indicating no dark toxicity. As expected, the ratio of green monomer to red complex gradually increased during longitudinal observation for 12 min in **BPD-MA**-treated cells, indicating the decline of $\Delta\psi_m$.[41] The modified compound **0323**, which previously showed the highest localization in the mitochondria and greatest singlet oxygen production, also exhibited the largest $\Delta\psi_m$ toxicity, which was significantly higher from 6 min onward ($p = 0.002$ at 6 min, $p < 0.0001$ at 8 min, $p < 0.0001$ at 10 min, and $p < 0.0001$ at 12 min) compared to **BPD-MA** (Figure 4k).

As expected, the mitochondria membrane potential was decreased after 690 nm irradiation in photosensitizer-treated KB cells and the magnitude of depolarization directly correlated with the extent of mitochondria localization. Thus, the compounds **BPD-MA** and **0323** had the greatest mitochondrial localization and the highest $\Delta\psi_m$ toxicity. As noted above, singlet oxygen species are short lived and have a diffusion radius of only 20 nm, requiring that the location in which they are produced also be the site where they cause the most damage. Consistent with this, the superior accumulation of **BPD-MA** and **0323** in the mitochondria agrees with the greater observed damage to $\Delta\psi_m$. Furthermore, our longitudinal study revealed a decline in membrane potential before mitochondria swelling,

DOI: 10.1021/acsomega.8b00692
ACS Omega 2018, 3, 6066–6074

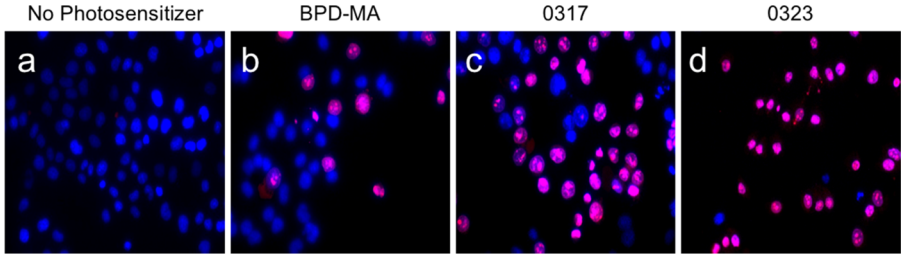

Figure 6. Modified compounds reduce cell viability following irradiation. KB cells were incubated for 1 h with either no photosensitizer or 50 nM **BPD-MA**, **0317**, or **0323** and exposed for 5 s to the NIR laser light. After 1 h, the cells were incubated with Hoechst dye (nuclear stain) and propidium iodide (vitality stain) before evaluation by fluorescence microscopy. (a–d) Merged images of Hoechst (blue) and propidium iodide (magenta) are shown, where dead cells appear magenta.

suggesting this phenomenon may be an event preceding early processes associated with apoptosis. Because the compound **0320** did not show a significant increase in SOS or change in $\Delta\psi_m$ in KB cells, this compound was not further studied.

Qualitative Changes: Actin, Mitochondria, and ROS Production. The next step in evaluating **BPD-MA** and its modified derivatives was to study the morphological changes in the cytoskeleton and mitochondria together with the production of reactive oxygen species (ROS) following irradiation. Nontreated cells displayed fibrous structures of actin filaments (Figure 5a), whereas **BPD-MA**-treated (Figure 5b), **0317**-treated (Figure 5c) and **0323**-treated (Figure 5d) cells showed fragmentation of the actin filaments. Importantly, **0317**-treated cells showed less fragmentation and more polymerized actin than **BPD-MA**- and **0323**-treated cells. Granular swelling of the mitochondria, which is a sign of cell damage, was also more prominent in **BPD-MA**-treated (Figure 5f) and **0323**-treated (Figure 5h) cells compared to control (Figure 5e) and **0317**-treated (Figure 5g) cells, which showed a normal tubular mitochondria structure. There was also an increase in ROS in **BPD-MA**-treated (Figure 5j), **0317**-treated (Figure 5k), and **0323**-treated (Figure 5l) cells compared to control cells (Figure 5i). Curiously, the greatest increase in reactive oxygen species was found to be in the nucleus, suggesting a significant effect of PDT on the reactive oxygen species production in the nucleus[42] and/or mitochondria nucleus retrograde signaling.[43] This prediction is supported by our finding of early signs of cell injury and pyknosis (next section)[44] upon initiation of PDT. Interestingly, **0323**-treated cells showed apoptotic bodies indicated by the arrow in Figure 5l, which will be investigated further in a section below.

We believe that the above chain of events begins with **0323** and **BPD-MA** localization in the mitochondria and their subsequent generation of reactive species, which then lead to mitochondrial membrane depolarization and loss of its integrity. Considering the integral role the mitochondrial membrane plays in the regulation of electrolyte balance,[45] its deterioration can be expected to bring about a charge imbalance that will cause mitochondria swelling. The mitochondria membrane potential is crucial for ATP production through oxidative phosphorylation.[45] Actin assembly and disassembly, which are essential for the structural integrity of the cell,[46] molecular signaling within the cell,[47] and mitochondria motility,[48,49] are dependent on ATP for their regulation. Therefore, damaging the $\Delta\psi_m$ will lead to its depolymerization, as shown in this study.

Analysis of Cell Death. Viability assays were then performed using propidium iodide on photosensitizer-treated KB cells irradiated with 690 nm light. Four different treatment groups were examined, namely a control group, which consisted of KB cells treated with no photosensitizer (Figure 6a) and treated groups preincubated with **BPD-MA** (Figure 6b), **0317** (Figure 6c) or **0323** (Figure 6d). As shown in Figure 6, after irradiation, propidium iodide staining was only observed in photosensitizer-treated cells, with **0323** showing the greatest cytotoxicity (93% PI positive), **0317** demonstrating an intermediate toxicity (54% positive), and **BPD-MA** displaying the lowest cytotoxicity (25% positive). Pyknosis, which involves an irreversible condensation of chromatin, was also observed.

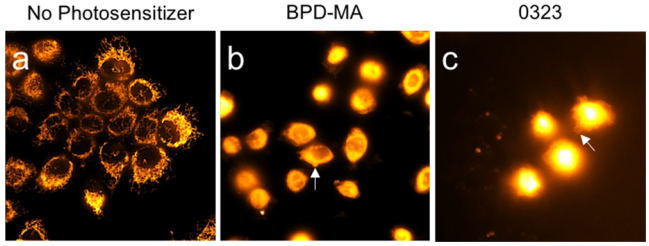

Figure 7. Induction of apoptosis following PDT. (a) Cytochrome *C* localization in KB cells with no photosensitizer. Cytochrome *C* release in **BPD-MA**-treated (b) and **0323**-treated (c) cells. Arrows indicate apoptotic bodies.

Apoptosis Through Cytochrome *C* Release from the Mitochondria. Considering the roles of mitochondria damage[50] and actin network disassembly[51] in mediating apoptosis, we evaluated the most effective photosensitizer to this point (**0323**) and the parent compound (**BPD-MA**) for the release of cytochrome *C* as a measure of one of the hallmarks of apoptosis. Two major mechanisms of cell death consist of necrosis and apoptosis. Apoptosis is desirable in PDT because it minimizes inflammation to adjacent normal tissue.[52] One of the first events that occurs in apoptosis is the release of cytochrome *C* from the inner membrane of the mitochondria to the cytosol.[53] Whereas release of cytochrome *C* from mitochondria was prominent in **BPD-MA**-treated (Figure 7b) and **0323**-treated (Figure 7c) cells, little if any cytochrome *C* release was observed from the mitochondria in control cells (Figure 7a). This is consistent with previous studies, which have shown that **BPD-MA** induces apoptosis.[54,55] Moreover, apoptotic bodies, which are hallmarks of cell apoptosis,[56] can be observed in the photosensitizer-treated groups (see arrows). Another function of cytochrome *C* upon release from the mitochondria is to induce chromatin condensation following its translocation to the nucleus.[57] Interestingly, cytochrome *C* is localized more in the nucleus of **0323**-treated cells than in **BPD-MA**-treated cells. This study shows PDT with the

DOI: 10.1021/acsomega.8b00692
ACS Omega 2018, 3, 6066–6074

modified compound **0323** induces apoptosis similar to **BPD-MA**.

CONCLUSIONS

In conclusion, we have developed a mitochondria-targeted photosensitizer by adding a triphenylphosphine (TPP^+) group to carboxyl terminus of the parent PDT agent, verteporfin (**0323**). This mitochondria-targeting moiety was more efficacious than monoguanidium (**0317**) or bis-guanidinium (**0320**) in targeting the mitochondria. Improving the mitochondria localization of verteporfin resulted in increased singlet oxygen species (SOS), depolarization of mitochondria membrane potential, and cell death. Moreover, elevated actin depolymerization, increased reactive oxygen species, enhanced mitochondria swelling, pyknosis, and apoptosis were also observed. Based on these observations, we recommend tethering a TPP moiety to the desired PDT agent when developing a photosensitizer for cytotoxic applications.

EXPERIMENTAL SECTION

Chemicals and Materials. 2-(1*H*-7-Azabenzotriazol-1-yl)-1,1,3,3-tetramethyl uronium hexafluorophosphate methanaminium (HATU) was obtained from Genscript Inc. (Piscataway, New Jersey). Guanidine hydrochloride, 1,2-dichloro ethane (1,2-DCE), diisopropylethylamine (DIPEA), dimethyl sulfoxide (DMSO), and all other reagents were purchased from Sigma-Aldrich. Trimethyltin hydroxide (Me_3SnOH) was purchased from Alfa Aesar. For the synthesis of **0323**, (2-aminoethyl)triphenylphosphonium bromide was synthesized according to reported procedures.[29,30]

Synthesis of Mono/Bicationic Derivatives of Verteporfin. For synthesis of mitochondria targeted monocationic derivatives of verteporfin (1 equiv) dissolved in anhydrous DMSO containing diisopropylethylamine (5 equiv) and HATU (1 equiv) were stirred for 30 min under argon atmosphere. To obtain **0317** and **0323**, 3-fold molar excess of guanidine hydrochloride salt and 3-fold molar excess of (2-aminoethyl)-triphenylphosphonium bromide, respectively, were then added and stirred overnight at room temperature, as outlined in Figure 1. The crude products were purified by preparative reverse phase high-performance liquid chromatography (HPLC) using a mobile phase of A = 20 mM ammonium acetate buffer, pH 7; B = acetonitrile; gradient 0−50% B in 30 min, 13 mL min^{-1}, λ = 280 nm. Pure fractions were analyzed by LCMS and (see Figure S2 in the Supporting Information) pooled and lyophilized to furnish **0317** and **0323**.

For synthesis of the polycationic derivatives of verteporfin, we used Me_3SnOH reagent for mild methyl ester hydrolysis of verteporfin. Verteporfin (1 equiv) dissolved in anhydrous 1,2-DCE containing Me_3SnOH (10 equiv) was stirred for 1 h at 80 °C. The reaction was monitored by LCMS and the crude product was purified by preparative reverse-phase HPLC using a mobile phase of A = 20 mM ammonium acetate buffer, pH 7; B = acetonitrile; gradient 0−50% B in 30 min, 13 mL min^{-1}, λ = 280 nm. The methyl ester hydrolyzed verteporfin (1 equiv) dissolved in anhydrous DMSO containing diisopropylethylamine (5 equiv) and HATU (1 equiv) was stirred for 30 min under argon atmosphere. A 10-fold molar excess of guanidine hydrochloride salt was then added and stirred overnight at room temperature, as outlined in Figure 1. The crude product was purified by preparative reverse-phase HPLC using a mobile phase of A = 20 mM ammonium acetate buffer, pH 7; B = acetonitrile; gradient 0−50% B in 30 min, 13 mL min^{-1}, λ = 280 nm. Pure fractions were analyzed by LCMS and (see Figure S3 in the Supporting Information) pooled and lyophilized to furnish **0320**. The measured extinction coefficients of the aforementioned PDT agents were found to be 3.5×10^4 M^{-1} cm^{-1} (**BPD-MA**), 2.4×10^4 M^{-1} cm^{-1} (**0317**), and 2.2×10^4 M^{-1} cm^{-1} (**0323**).

Cell Culture, Plating. KB cells were cultured with 5 mL of folic acid (−) RPMI media (Gibco) with 5% fetal bovine serum (FBS) (Atlanta biologicals) and 1% penicillin/streptomycin (GIbco) in 25 mL cell culture flasks (Corning, Sigma-Aldrich). Splitting was done 2−3 times per week or when cell culture flasks reached about 90% confluence. Cells were plated on 4-well chambers (Nunc Lab-Tek Chamber Slide System) in 500 μL media and allowed to grow for 2−3 days or when plates reached 90% confluence. Due to the nature of photosensitizers, all drug and dye incubations were done in the dark.

Colocalization Experiment. Following cell plating, the cells were co-incubated with 50 nM drug and 15 nM Mitotracker green (obtained from Life Technologies) for 1 h in RPMI media. The cells were then washed two times with phosphate-buffered saline (PBS) and kept in CO_2-independent media (Life technologies) for imaging. Because the excitation of the drug may cause morphological changes in the mitochondria within seconds, Mitotracker green was captured first at 488/520 nm and photosensitizers were captured at 690 nm.

Singlet Oxygen Experiment. The cells were co-incubated with 50 nM drug and 10 μM singlet oxygen sensor green (SOSG, Life Technologies) for 1 h in FBS (−) MEM. They were washed two times with PBS and kept in CO_2-independent media for imaging. The cells were then irradiated with 690 nm light followed by SOSG capture at 488/520 nm.

Mitochondria Membrane Potential Experiment. The cells were incubated with 50 nM **BPD-MA**, **0317**, **0320**, or **0323** in RPMI for 1 h followed by two washes with PBS. They were then incubated in 7.665 μM JC-1 (a probe of mitochondrial membrane potential; Life Technologies) in RPMI for 10 min followed by two washes with PBS and kept in CO_2-independent media. JC-1 was captured before irradiation at 590 nm (J-aggregates) and 529 nm (green monomers). The cells were then irradiated with 690 nm light. JC-1 was immediately captured at 590 and 529 nm at 2 min intervals for 12 min.

Cytoskeleton and Mitochondria Structure Experiment. The cells were incubated with 50 nM **BPD-MA**, **0317**, or **0323** in RPMI for 1 h followed by two washes with PBS and kept in CO_2-independent media. They were then irradiated using 690 nm light. Cells were then fixed with 4% PFA for 15 min, permeabilized with 1% Triton X-100 for 30 min and blocked with goat kit[31] for 60 min. The cells were then stained with F-actin green labeling kit (Life Technologies) for 30 min, 1 μM Mitotracker deep-red FM (Life Technologies) for 30 min, and 1 μg mL^{-1} Hoechst for 30 min. They were then washed two times with PBS and images were captured at 520 nm for actin, 461 nm for Hoechst, and 665 nm for mitochondria stain.

ROS Experiment. The cells were incubated with 50 nM **BPD-MA**, **0317**, or **0323** in RPMI for 1 h followed by two washes with PBS. They were then incubated with 5 μM ROS in RPMI for 30 min followed by two washes with PBS and kept in CO_2-independent media. The cells were irradiated with 690 nm light and ROS were captured at 488/520 nm.

DOI: 10.1021/acsomega.8b00692
ACS Omega 2018, 3, 6066−6074

Cell Death Experiment. The KB cells were incubated with 50 nM of **BPD-MA**, **0317**, or **0323** diluted in RPMI media for 1 h. They were washed two times with PBS (Gibco), followed by irradiation for 5 s by the NIR laser light. After 1 h, the cells were incubated with 5 μg mL^{-1}Hoechst dye (nuclear stain) and 1 μg mL^{-1}propidium iodide (vitality stain) for 30 min. The cells were then washed two times with PBS, kept in CO_2-independent media, and then imaged at 350/461 and 535/617 nm for Hoechst and propidium iodide dyes, respectively.

Apoptosis Experiment. The cells were incubated with 50 nM **BPD-MA** or **0323** in RPMI for 1 h followed by two washes with PBS and kept in CO_2-independent media. They were then irradiated using 690 nm light and then incubated at 37 °C and 5% CO_2 for 2 days. The cells were then fixed using 4% PFA for 15 min, permeablized using 1% Triton X-100 for 30 min, and blocked with a goat kit to prevent nonspecific binding for 30 min. They were then stained with 5 μg mL^{-1} mouse IgG anti-cytochrome *C* (BioLegend) for 20 h and washed three times with PBS. The cells were then counterstained with Alexa Fluor 594 Goat antimouse antibody (594) for 90 min and washed three times with PBS. Cytochrome *C* was then captured using 617 nm emission wavelength.

Microscopy and Imaging Analysis. Images were taken using Nikon Ti-S epifluorescence microscope equipped with incubating chamber set at 37 °C and an oil immersion 60× objective, and the images were obtained with NIS-Elements software. Colocalization analysis was done using the JACoP plugin tool in Fiji ImageJ to calculate the Pearson's correlation coefficient. Singlet oxygen production analysis was done using ImageJ to obtain SOSG intensities. Fluorescence intensity map was obtained using ImageJ. Mitochondria membrane potential analysis was also done using ImageJ to calculate green-to-red channel intensity ratio. For ImageJ analysis, the region of interest feature was selected to precisely quantify the mean gray value intensity of each cell.

Statistics. Statistical analysis was performed using Prism 7. One-way and two-way ANOVA were used to compare the population mean of different treatment groups at 0.05 significant level. Tukey post-hoc test was further applied to determine the statistical significance of mean difference among the groups.

■ ASSOCIATED CONTENT

Supporting Information

The Supporting Information is available free of charge on the ACS Publications website at DOI: 10.1021/acsomega.8b00692.

LCMS characterization of the isomeric mixtures of **BPD-MA**, **0323**, and **0320** (PDF)

■ AUTHOR INFORMATION

Corresponding Author

*E-mail: plow@purdue.edu.

ORCID

Philip S. Low: 0000-0001-9042-5528

Present Address

‖Indiana University School of Medicine, Indianapolis, Indiana 46202, United States (J.O.)

Author Contributions

⊥S.M.M. and J.O. contributed equally.

Notes

The authors declare no competing financial interest.

■ ACKNOWLEDGMENTS

This work was supported in part by a grant from On Target Laboratories.

■ REFERENCES

(1) Dolmans, D. E. J. G. J.; Fukumura, D.; Jain, R. Photodynamic therapy for cancer. *Nat. Rev. Cancer* **2003**, *3*, 380−387.

(2) Henderson, B. W.; Dougherty, T. J. How does photodynamic therapy work? *Photochem. Photobiol.* **1992**, *55*, 145−157.

(3) Foote, C. S. Definition of type I and type II photosensitized oxidation. *Photochem. Photobiol.* **1991**, *54*, 659.

(4) Wilkinson, F.; Helman, W. P.; Ross, A. B. Quantum Yields for the Photosensitized Formation of the Lowest Electronically Excited Singlet State of Molecular Oxygen in Solution. *J. Phys. Chem. Ref. Data* **1993**, *22*, 113−262.

(5) Oliveira, C. S.; Turchiello, R.; Kowaltowski, A. J.; Indig, G. L.; Baptista, M. S. Major determinants of photoinduced cell death: Subcellular localization versus photosensitization efficiency. *Free Radical Biol. Med.* **2011**, *51*, 824−33.

(6) Moan, J.; Berg, K. The photodegradation of porphyrins in cells can be used to estimate the lifetime of singlet oxygen. *Photochem. Photobiol.* **1991**, *53*, 549−553.

(7) Redmond, R. W.; Kochevar, I. E. Spatially resolved cellular responses to singlet oxygen. *Photochem. Photobiol.* **2006**, *82*, 1178−1186.

(8) Rubio, N.; Fleury, S. P.; Redmond, R. W. Spatial and temporal dynamics of in vitro photodynamic cell killing: extracellular hydrogen peroxide mediates neighbouring cell death. *Photochem. Photobiol. Sci.* **2009**, *8*, 457−464.

(9) Kurokawa, H.; Ito, H.; Inoue, M.; Tabata, K.; Sato, Y.; Yamagata, K.; et al. High resolution imaging of intracellular oxygen concentration by phosphorescence lifetime. *Sci. Rep.* **2015**, *5*, No. 10657.

(10) Green, D. R.; Reed, J. C. Mitochondria and apoptosis. *Science* **1998**, *281*, 1309−1312.

(11) Hoye, A. T.; Davoren, J. E.; Wipf, P.; Fink, M. P.; Kagan, V. E. Targeting Mitochondria. *Acc Chem. Res.* **2008**, *41*, 87−97.

(12) Chen, J. Y.; Mak, N. K.; Yow, C. M.; Fung, M. C.; Chiu, L. C.; Leung, W. N.; et al. The binding characteristics and intracellular localization of temoporfin (mTHPC) in myeloid leukemia cells: phototoxicity and mitochondrial damage. *Photochem. Photobiol.* **2000**, *72*, 541−547.

(13) Wilson, B. C.; Olivo, M.; Singh, G. Subcellular localization of Photofrin and aminolevulinic acid and photodynamic cross-resistance in vitro in radiation-induced fibrosarcoma cells sensitive or resistant to photofrin-mediated photodynamic therapy. *Photochem. Photobiol.* **1997**, *65*, 166−176.

(14) Celli, J. P.; Solban, N.; Liang, A.; Pereira, S.; Hasan, T. Verteporfin-Based Photodynamic Therapy Overcomes Gemcitabine Insensitivity in a Panel of Pancreatic Cancer Cell Lines. *Lasers Surg. Med.* **2011**, *43*, 565−574.

(15) Sibrian-Vazquez, M.; Nesterova, I. V.; Jensen, T. J.; Vicente, M. G. H. Mitochondria Targeting by Guanidine− and Biguanidine−Porphyrin Photosensitizers. *Bioconjugate Chem.* **2008**, *19*, 705−713.

(16) Cheng, G.; Zielonka, J.; Ouari, O.; Lopez, M.; McAllister, D.; Boyle, K.; et al. Mitochondria-Targeted Analogues of Metformin Exhibit Enhanced Antiproliferative and Radiosensitizing Effects in Pancreatic Cancer Cells. *Cancer Res.* **2016**, *76*, 3904−3915.

(17) Millard, M.; Gallagher, J. D.; Olenyuk, B. Z.; Neamati, N. A selective mitochondrial-targeted chlorambucil with remarkable cytotoxicity in breast and pancreatic cancers. *J. Med. Chem.* **2013**, *56*, 9170−9179.

(18) Hu, Q.; Gao, M.; Feng, G.; Liu, B. Mitochondria-targeted cancer therapy using a light-up probe with aggregation-induced-emission characteristics. *Angew. Chem., Int. Ed.* **2014**, *53*, 14225−14229.

(19) Liang, B.; Shao, W.; Zhu, C.; Wen, G.; Yue, X.; Wang, R.; et al. Mitochondria-Targeted Approach: Remarkably Enhanced Cellular Bioactivities of TPP2a as Selective Inhibitor and Probe toward TrxR. *ACS Chem. Biol.* **2016**, *11*, 425−434.

DOI: 10.1021/acsomega.8b00692
ACS Omega 2018, 3, 6066−6074

(20) Apostolova, N.; Victor, V. M. Molecular Strategies for Targeting Antioxidants to Mitochondria: Therapeutic Implications. *Antioxid. Redox Signaling* **2015**, *22*, 686−729.
(21) Dickinson, B. C.; Chang, C. J. A Targetable Fluorescent Probe for Imaging Hydrogen Peroxide in the Mitochondria of Living Cells. *J. Am. Chem. Soc.* **2008**, *130*, 9638−9639.
(22) Lv, W.; Zhang, Z.; Zhang, K. Y.; Yang, H.; Liu, S.; Xu, A.; et al. A Mitochondria-Targeted Photosensitizer Showing Improved Photodynamic Therapy Effects Under Hypoxia. *Angew. Chem., Int. Ed.* **2016**, *55*, 9947−9951.
(23) Zhang, C. J.; Hu, Q.; Feng, G.; Zhang, R.; Yuan, Y.; Lu, X.; et al. Image-guided combination chemotherapy and photodynamic therapy using a mitochondria-targeted molecular probe with aggregation-induced emission characteristics. *Chem. Sci.* **2015**, *6*, 4580−4586.
(24) Hu, Z.; Sim, Y.; Kon, O. L.; Ng, W. H.; Ribeiro, A. J. M.; Ramos, M. J.; et al. Unique Triphenylphosphonium Derivatives for Enhanced Mitochondrial Uptake and Photodynamic Therapy. *Bioconjugate Chem.* **2017**, *28*, 590−599.
(25) Zielonka, J.; Joseph, J.; Sikora, A.; Hardy, M.; Ouari, O.; Vasquez-Vivar, J.; et al. Mitochondria-Targeted Triphenylphosphonium-Based Compounds: Syntheses, Mechanisms of Action, and Therapeutic and Diagnostic Applications. *Chem. Rev.* **2017**, *117*, 10043−10120.
(26) Arnold, J.; Bauer, B.; Blumenkranz, M.; Bressler, N.; Bressler, S.; Chader, G.; et al. Guidelines for using verteporfin (Visudyne (R)) in photodynamic therapy to treat choroidal neovascularization due to age-related macular degeneration and other causes. *Retina* **2002**, *22*, 6−18.
(27) Bressler, N.; Roundtable, V.; Roundtable, V. Guidelines for using verteporfin (visudyne) in photodynamic therapy for choroidal neovascularization due to age related macular degeneration and other causes: Update. *Retina* **2005**, *25*, 119−134.
(28) Nicolaou, K. C.; Estrada, A. A.; Zak, M.; Lee, S. H.; Safina, B. S. A Mild and Selective Method for the Hydrolysis of Esters with Trimethyltin Hydroxide. *Angew. Chem., Int. Ed.* **2005**, *44*, 1378−1382.
(29) Maryanoff, B. E.; Reitz, A. B.; Duhl-Emswiler, B. A. Stereochemistry of the Wittig reaction. Effect of nucleophilic groups in the phosphonium ylide. *J. Am. Chem. Soc.* **1985**, *107*, 217−226.
(30) Jung, H. S.; Lee, J.; Kim, K.; Koo, S.; Verwilst, P.; Sessler, J. L.; Kang, C.; Kim, J. S. A Mitochondria-Targeted Cryptocyanine-Based Photothermogenic Photosensitizer. *J. Am. Chem. Soc.* **2017**, *139*, 9972−9978.
(31) Chen, Y.; Damayanti, N. P.; Irudayaraj, J.; Dunn, K.; Zhou, F. C. Diversity of two forms of DNA methylation in the brain. *Front. Genet.* **2014**, *5*, No. 46.
(32) Celli, J. P.; Solban, N.; Liang, A.; Pereira, S. P.; Hasan, T. Verteporfin-based photodynamic therapy overcomes gemcitabine insensitivity in a panel of pancreatic cancer cell lines. *Lasers Surg Med.* **2011**, *43*, 565−74.
(33) Fateye, B.; Wan, A.; Yang, X.; Myers, K.; Chen, B. Comparison between endothelial and tumor cells in the response to verteporfin-photodynamic therapy and a PI3K pathway inhibitor. *Photodiagn. Photodyn. Ther.* **2015**, *12*, 19−26.
(34) Gollmer, A.; Arnbjerg, J.; Blaikie, F. H.; Pedersen, B. W.; Breitenbach, T.; Daasbjerg, K.; et al. Singlet Oxygen Sensor Green: Photochemical Behavior in Solution and in a Mammalian Cell. *Photochem. Photobiol.* **2011**, *87*, 671−679.
(35) Choudhury, S. R.; Ordaz, J.; Lo, C. L.; Damayanti, N. P.; Zhou, F.; Irudayaraj, J. From the Cover: Zinc oxide Nanoparticles-Induced Reactive Oxygen Species Promotes Multimodal Cyto- and Epigenetic Toxicity. *Toxicol. Sci.* **2017**, *156*, 261−274.
(36) Waters, J. C. Accuracy and precision in quantitative fluorescence microscopy. *J. Cell Biol.* **2009**, *185*, 1135−1148.
(37) DeRosa, M.; Crutchley, R. Photosensitized singlet oxygen and its applications. *Coord. Chem. Rev.* **2002**, *233*−*234*, 351−371.
(38) Blokhina, O.; Virolainen, E.; Fagerstedt, K. Antioxidants, oxidative damage and oxygen deprivation stress: a review. *Ann. Bot.* **2003**, *91*, 179−194.
(39) Perelman, A.; Wachtel, C.; Cohen, M.; Haupt, S.; Shapiro, H.; Tzur, A. JC-1: alternative excitation wavelengths facilitate mitochondrial membrane potential cytometry. *Cell Death Dis.* **2012**, *3*, No. e430.
(40) Salido, M.; Gonzalez, J.; Vilches, J. Loss of mitochondrial membrane potential is inhibited by bombesin in etoposide-induced apoptosis in PC-3 prostate carcinoma cells. *Mol. Cancer Ther.* **2007**, *6*, 1292−1299.
(41) Perry, S. W.; Norman, J.; Barbieri, J.; Brown, E.; Gelbard, H. Mitochondrial membrane potential probes and the proton gradient: a practical usage guide. *BioTechniques* **2011**, *50*, 98−115.
(42) Provost, C.; Choufani, F.; Avedanian, L.; Bkaily, G.; Gobeil, F.; Jacques, D. Nitric oxide and reactive oxygen species in the nucleus revisited. *Can. J. Physiol. Pharmacol.* **2010**, *88*, 296−304.
(43) Kotiadis, V. N.; Duchen, M.; Osellame, L. Mitochondrial quality control and communications with the nucleus are important in maintaining mitochondrial function and cell health. *Biochim. Biophys. Acta, Gen. Subj.* **2014**, *1840*, 1254−1265.
(44) Vinay, K.; Abbas, A. K.; Fausto, N. *Robbins and Cotran Pathologic Basis of Disease*; Elsevier Saunders: Philadelphia, 2014.
(45) Hüttemann, M.; Lee, I.; Pecinova, A.; Pecina, P.; Przyklenk, K.; Doan, J. Regulation of oxidative phosphorylation, the mitochondrial membrane potential, and their role in human disease. *J. Bioenerg. Biomembr.* **2008**, *40*, 445−456.
(46) Stricker, J.; Falzone, T.; Gardel, M. Mechanics of the F-actin cytoskeleton. *J. Biomech.* **2010**, *43*, 9−14.
(47) Obrdlik, A.; Kukalev, A.; Louvet, E.; Farrants, A.-K.; Caputo, L.; Percipalle, P. The histone acetyltransferase PCAF associates with actin and hnRNP U for RNA polymerase II transcription. *Mol. Cell. Biol.* **2008**, *28*, 6342−6357.
(48) Boldogh, I. R.; Pon, L. Interactions of mitochondria with the actin cytoskeleton. *Biochim. Biophys. Acta, Mol. Cell Res.* **2006**, *1763*, 450−462.
(49) Olson, E. N.; Nordheim, A. Linking actin dynamics and gene transcription to drive cellular motile functions. *Nat. Rev. Mol. Cell Biol.* **2010**, *11*, 353−365.
(50) Wang, C.; Youle, R. J. The Role of Mitochondria in Apoptosis. *Annu. Rev. Genet.* **2009**, *43*, 95−118.
(51) Desouza, M.; Gunning, P. W.; Stehn, J. R. The actin cytoskeleton as a sensor and mediator of apoptosis. *Bioarchitecture* **2012**, *2*, 75−87.
(52) Fink, S. L.; Cookson, B. T. Apoptosis, Pyroptosis, and Necrosis: Mechanistic Description of Dead and Dying Eukaryotic Cells. *Infect. Immun.* **2005**, *73*, 1907−1916.
(53) Ott, M.; Robertson, J. D.; Gogvadze, V.; Zhivotovsky, B.; Orrenius, S. Cytochrome c release from mitochondria proceeds by a two-step process. *Proc. Natl. Acad. Sci. U.S.A.* **2002**, *99*, 1259−1263.
(54) Granville, D. J.; Levy, J.; Hunt, D. Photodynamic treatment with benzoporphyrin derivative monoacid ring A produces protein tyrosine phosphorylation events and DNA fragmentation in murine P815 cells. *Photochem. Photobiol.* **1998**, *67*, 358−362.
(55) Granville, D. J.; Levy, J. G.; Hunt, D. W. Photodynamic therapy induces caspase-3 activation in HL-60 cells. *Cell Death Differ.* **1997**, *4*, 623−628.
(56) Jiang, X.; Wang, X. Cytochrome C-mediated apoptosis. *Annu. Rev. Biochem.* **2004**, *73*, 87−106.
(57) Nur-E-Kamal, A.; Gross, S. R.; Pan, Z.; Balklava, Z.; Ma, J.; Liu, L. F. Nuclear Translocation of Cytochrome c during Apoptosis. *J. Biol. Chem.* **2004**, *279*, 24911−24914.

DOI: 10.1021/acsomega.8b00692
ACS Omega 2018, 3, 6066−6074